Article

Cell Reports

The Ovulatory Signal Precipitates LRH-1 Transcriptional Switching Mediated by Differential Chromatin Accessibility

Graphical Abstract

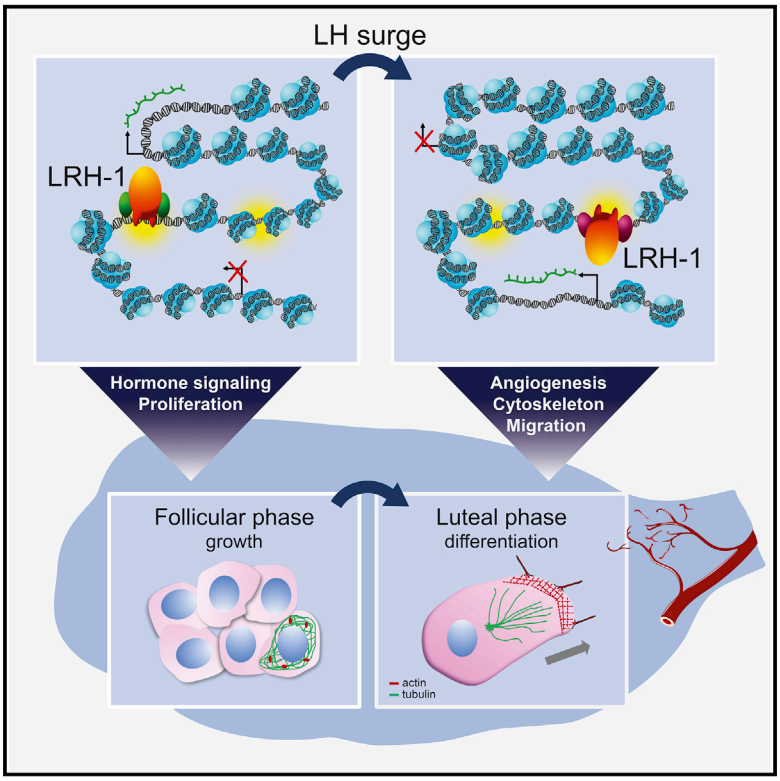

Highlights

- The LH signal initiates extensive chromatin remodeling in the ovarian follicle
- LRH-1-specific DNA sequence motifs are found in open chromatin domains
- Dynamic LRH-1 cistrome reprogramming controls granulosa cells differentiation
- LRH-1 directly regulates early events leading to ovulation

Authors

Stéphanie Bianco, Anne-Marie Bellefleur, Élaine Beaulieu, ..., Kristina Schoonjans, Bruce D. Murphy, Nicolas Gévry

Correspondence

nicolas.gevry@usherbrooke.ca

In Brief

Bianco et al. evaluate chromatin accessibility, LRH-1 ChIP-seq, and RNA-seq to establish early events in ovarian follicles following the LH surge leading to ovulation. They demonstrate extensive chromatin remodeling and reprogramming of the LRH-1 cistrome and transcriptome. CRE-lox depletion of LRH-1 prevents key ovulatory processes, including cell migration and angiogenesis.

Bianco et al., 2019, Cell Reports *28*, 2443–2454
August 27, 2019
https://doi.org/10.1016/j.celrep.2019.07.088

CellPress

Cell Reports
Article

The Ovulatory Signal Precipitates LRH-1 Transcriptional Switching Mediated by Differential Chromatin Accessibility

Stéphanie Bianco,[1] Anne-Marie Bellefleur,[2,5] Élaine Beaulieu,[1,6] Charles Joly Beauparlant,[3] Kalyne Bertolin,[2,7] Arnaud Droit,[3] Kristina Schoonjans,[4] Bruce D. Murphy,[2,8] and Nicolas Gévry[1,8,9,*]

[1]Département de biologie, Faculté des sciences, Université de Sherbrooke, Sherbrooke, QC J1K 2R1, Canada
[2]Centre de recherche en reproduction et fertilité, Faculté de médecine vétérinaire, Université de Montréal, Saint-Hyacinthe, QC J2S 2M2, Canada
[3]Centre de Recherche du CHU de Québec, Université Laval, Département de médecine moléculaire, Faculté de médecine, QC G1V 4G2, Canada
[4]Laboratory of Metabolic Signaling, École polytechnique fédérale de Lausanne, 1015 Lausanne, Switzerland
[5]Present address: L'Alliance Boviteq Inc., Saint-Hyacinthe, QC J2T 5H1, Canada
[6]Present address: Department of Biology, University of Ottawa, Gendron Hall, Ottawa, ON K1N 6N5, Canada
[7]Present address: Programa de Pós-Graduação em Medicina Veterinária, Universidade Federal de Santa Maria, Santa Maria RS 97105-900, Brazil
[8]These authors contributed equally
[9]Lead Contact
*Correspondence: nicolas.gevry@usherbrooke.ca
https://doi.org/10.1016/j.celrep.2019.07.088

SUMMARY

In the ovary, follicular growth and maturation are complicated processes that involve a series of morphological and physiological changes in oocytes and somatic cells leading to ovulation and luteinization, essential processes for fertility. Given the complexity of ovulation, characterization of genome-wide regulatory elements is essential to understand the mechanisms governing the expression of specific genes in the rapidly differentiating follicle. We therefore employed a systems biology approach to determine global transcriptional mechanisms during the early stages of the ovulatory process. We demonstrate that, following the hormonal signal that initiates ovulation, granulosa cells undergo major modification of distal regulatory elements, which coincides with cistrome reprogramming of the indispensable orphan nuclear receptor liver receptor homolog-1 (LRH-1). This cistromic reorganization correlates with the extensive changes in gene expression in granulosa cells leading to ovulation. Together, our study yields a highly detailed transcriptional map delineating ovarian cell differentiation during the initiation of ovulation.

INTRODUCTION

The developmental trajectory of the mammalian female gamete begins prior to birth, when the oocyte becomes encased in the granulosa cells of the primordial follicle (Pepling, 2012). Subsequent events, under the regulation of multiple factors, lead to the development of the follicle to the preovulatory stage (Binelli and Murphy, 2010). The pituitary signal, in the form of a luteinizing hormone (LH) surge, serves as the trigger to provoke ovulation of the follicle (Duggavathi and Murphy, 2009). This signal launches an intensive program of cellular differentiation, orchestrated by major changes in the transcriptional profile of the follicular granulosa cells, culminating in the expulsion of the oocyte (Duggavathi and Murphy, 2009). Remodeling granulosa cells includes, among others, introduction of vascularity into the follicle, cell migration, massive changes in cholesterol importation and steroid secretion, and terminal differentiation to the luteal phenotype (Fan et al., 2011).

The liver receptor homolog-1 (LRH-1) is an orphan nuclear receptor coded by the *Nr5a2* gene that is expressed in the ovary, specifically in granulosa cells of all follicle classes, from primordial through preovulatory, and in the differentiated granulosa cells in the corpus luteum (Meinsohn et al., 2019). Our previous studies with conditional knockout (cKO) models have shown important role of LRH-1 in the ovulatory process. Depletion of LRH-1 from granulosa cells, by means of crossing LRH-1 floxed mice with mice expressing the anti-Müllerian hormone receptor-2 (*Amhr2*) Cre recombinase, was employed to excise two exons of the LRH-1 gene in primary and all later-stage follicles (Duggavathi et al., 2008). The same floxed mouse was bred with the aromatase cytochrome P450 family 19 subfamily A polypeptide 1 (*Cyp19a1*) Cre mouse for excision in antral and later follicles (Bertolin et al., 2014). In both studies, large preovulatory follicles were formed, but no ovulation occurred. When depletion was achieved using progesterone receptor (*Pgr*) Cre, expressed after the ovulatory signal, ovulation was not affected (Zhang et al., 2013), clearly demonstrating the crucial role of LRH-1 in directing ovulation. However, little is known about the molecular aspects of LRH-1 regulation of ovulatory remodeling of the follicle.

It is known that key genes that are modified following the LH signal include those required for steroid synthesis, cholesterol

mobilization, cell proliferation, prostaglandin synthesis, and expansion of the cumulus oöphorus (Bertolin et al., 2014, 2017; Duggavathi et al., 2008; Meinsohn et al., 2017). Nonetheless, the large-scale modification of the transcriptome that directs ovulatory remodeling engenders synchronization of multiple, hierarchic processes, mandating a systems approach to determining the global chromatin landscape and the molecular dynamics of ovulation. The widespread and varied influence of LRH-1 points to its significance in the process at several levels, including acting as a transcription factor, binding to promotor regions upstream of transcription start sites (Fayard et al., 2004) or to enhancers, acting at regions distal to target genes (Bianco et al., 2014). A similar example of extensive transcriptional reprogramming is that associated with the establishment of mammalian induced pluripotent stem cells (iPSCs). It has been shown that this process engenders the widespread modification of nucleosome occupancy and regions of open chromatin to allow for binding of the regulatory transcription factors that drive the transcriptional agenda for dedifferentiation (Li et al., 2017). Recently, the chromatin signature that concurs with transcriptional reprogramming that occurs during reactivation of silenced somatic cell genes in the *Xenopus* oocyte was explored (Miyamoto et al., 2018). These authors reported that chromatin accessibility is a central factor that allows the successful transcriptional reprogramming of oocytes.

In the present study, we used a systems approach to address the complexity of ovulation in a mouse model. Formaldehyde-assisted isolation of regulatory elements combined with next-generation sequencing (FAIRE-seq) (Bianco et al., 2015; Simon et al., 2012) was employed to map genome-wide chromatin accessibility of regulatory elements of granulosa cells before and after the ovulatory signal, revealing a dynamic remodeling of chromatin accessibility for transcription factors. We then examined genome-wide binding of LRH-1 using chromatin immunoprecipitation combined with next-generation sequencing (ChIP-seq) to determine its potential transcriptional targets in the early events following the LH signal. The transcriptomes of wild-type and Amhr2Cre/LRH-1 floxed mice (cKO) (Duggavathi et al., 2008) were explored by RNA sequencing, to show stage-specific gene expression programs controlled by LRH-1 before and after the LH signal. This integrated, multi-omics analysis exposed an extensive and specific LRH-1 regulatory network directing the early events of ovulation. Together, these results revealed that hormonal stimulation of the preovulatory follicle activates an LRH-1 transcriptional switch, thereby modulating multiple processes that included the cytoskeletal remodeling and cell migration essential for ovulation and luteinization.

RESULTS

The Ovulatory Signal Induces Important Reprogramming of Regulatory Elements in Granulosa Cells

Using a standard ovulation induction protocol, immature mice were injected with equine chorionic gonadotropin (eCG) to stimulate preovulatory follicle maturation, followed 44 h later by an injection of the LH congener human chorionic gonadotropin (hCG) to initiate ovulation (the ovulatory signal [OvS]; Figure 1A). In this protocol, ovulation occurs ~12 h after hCG injection, resulting in terminal differentiation of granulosa cells and expulsion of the oocyte from the follicle. We focused our analysis on the molecular events of the early stage before and after the OvS, at 0 h (hereafter −OvS) and at 4 h post-hCG (hereafter +OvS).

To identify genome-wide transcriptional regulatory elements before and after the OvS, we performed FAIRE-seq on granulosa cells isolated from ovaries. We observed that granulosa cells underwent major reprogramming of regulatory elements after the OvS. Indeed, 32,735 FAIRE-enriched regions were identified, with 25% (8,293 FAIRE sites) of them showing an increase in FAIRE-seq signal following OvS (hereafter referred as +OvS specific), 23% (7,570 FAIRE sites) showing a decrease (hereafter referred as −OvS specific), and 52% (16,872 FAIRE sites) remaining unchanged (hereafter referred as common) (Figures 1B, 1C, S2A, and S2B). Remarkably, most regulatory elements, particularly those specific either to the −OvS or +OvS stages, were associated with intragenic and distal intergenic regions, suggesting that these regions may be pivotal in the transcriptional regulation of granulosa cell differentiation (Figure 1D).

To identify the biological networks linked to these stage-specific regions, we performed a Genomic Region Enrichment of Annotation Tool (GREAT) analysis (McLean et al., 2010). Interestingly, we found that +OvS-specific regulatory elements were associated with signaling pathways linked to ovarian follicular growth and differentiation, such as the transforming growth factor β (TGF-β) and vascular endothelial growth factor (VEGF) pathways and adherens junctions (Figure 1E; Table S1). GREAT analysis also highlighted a specific expression signature of the gonadotropin releasing hormone (GnRH) pathway in granulosa cells (Table S1). In contrast, −OvS-specific FAIRE sites were found to be associated with pathways involved in hormone synthesis, apoptosis, and immune system activation. Finally, enriched FAIRE sites that remained common before and after the OvS were most frequently found in promoter regions and coincided with genes involved in basic cellular mechanisms, such as RNA processing, regulation of transcription, and protein processing (Figures 1D and 1E; Table S1). Together, these results highlight the biological relevance of the −OvS-specific and +OvS-specific accessibility profiles in the understanding of complex dynamic processes that drive changes in ovarian gene expression that are critical for ovulation.

Granulosa Cell Open Chromatin Domains Contain Stage-Specific DNA Sequence Motifs

The dramatic changes in DNA accessibility after the ovulatory stimulus described above are indicative of the binding of specific transcription factors to these regions. To identify potential transcription factors associated to −OvS and +OvS stage-specific transcription, we performed DNA motif discovery analysis using the Hypergeometric Optimization of Motif EnRichment (HOMER) bioinformatic approach (Heinz et al., 2010). We determined the top 10 motifs that were significantly enriched in each stage-specific FAIRE-seq cluster (Figure 2A; Table S2). Common FAIRE peaks were enriched in CTCF factors and specific transcription regulators such as SP1, NFY, or KLF5, which have been shown to be commonly associated with promoter regions (Kaczynski et al., 2003; Suske, 2017). Open chromatin regions that became

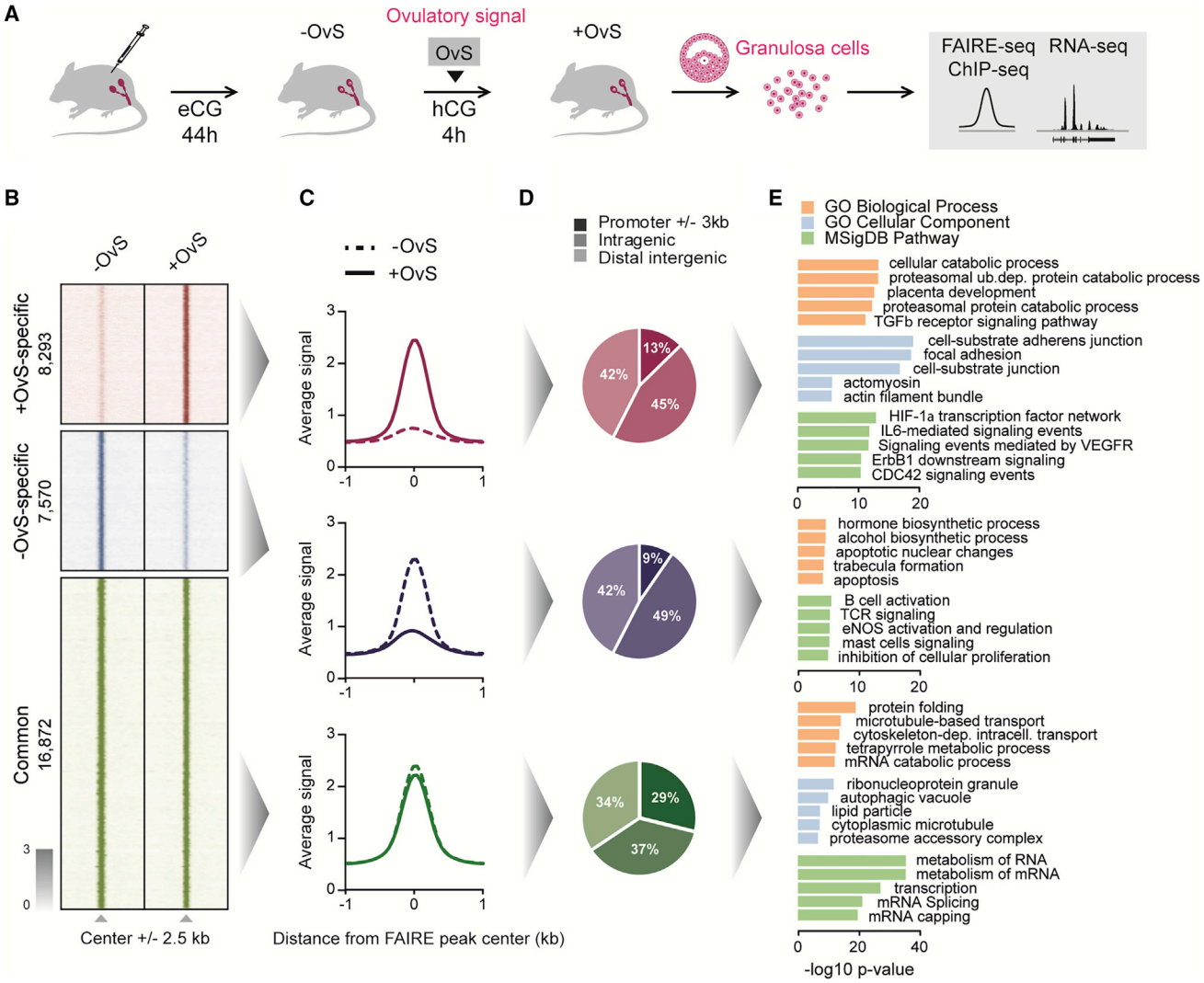

Figure 1. The Ovulatory Hormonal Signal Induces Large-Scale Reprogramming of Regulatory Elements in Granulosa Cells

(A) Schematic overview of mouse model showing the stimulation protocol and genomic approach used to identify regulatory elements involved in transcription during terminal differentiation of ovarian granulosa cells. Granulosa cells were purified from ovary before (−OvS) and after (+OvS) the ovulatory signal. Immature mice were injected intraperitoneally with equine chorionic gonadotropin (eCG) to stimulate follicular development, followed by injection of human chorionic gonadotropin (hCG) 44 h post-eCG, to induce ovulation. At 4 h post-hCG, pure granulosa cells were aspirated for FAIRE-seq (formaldehyde-assisted isolation of regulatory elements) and RNA-seq analysis.

(B) Heatmap showing the normalized FAIRE-seq signals (±OvS) centered on the 32,735 FAIRE-seq enriched regions (±2.5 kb) subdivided according to their dynamic status following OvS, i.e., the +OvS-specific regions showing an increase in FAIRE-seq signal, the −OvS-specific regions showing a decrease, and the common or unchanged regions.

(C) Aggregated signal profiles of +OvS-specific, −OvS-specific, and common FAIRE peaks in the 1-kb window around the FAIRE peak center. Dotted line represents the FAIRE signal before the OvS and the full line represents the signal after the OvS.

(D) Genomic distribution of FAIRE peaks before and after the OvS in granulosa cells.

(E) GO term analysis of genes associated with stage-specific open chromatin regions.

See also Figure S1 and Table S1.

less accessible after the OvS also harbored CTCF DNA motifs. CTCF regulates enhancer-promoter interactions and contributes to the three-dimensional organization of the genome (Arzate-Mejía et al., 2018). Our results therefore suggest that CTCF may have a role in granulosa cell stage-specific genome organization. Furthermore, these −OvS-specific FAIRE sites were also enriched in DNA motifs of transcription factors known to be involved in hormone signaling, such as GATA and GR. For the +OvS-specific FAIRE sites, the AP-1 transcription factor members (JUN, FOS, and ATF family) were the most frequently enriched motifs, a result in agreement with a previous report that showed the importance of these factors in the transition of proliferating granulosa cells to terminally differentiated cells following the OvS (Sharma and Richards, 2000). Moreover, it

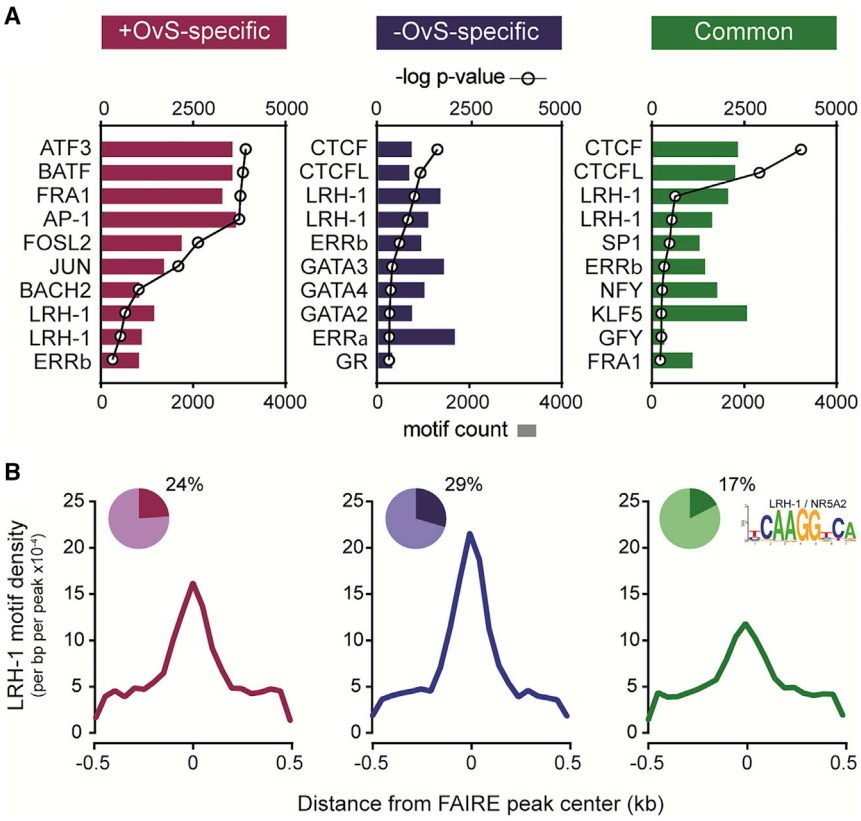

Figure 2. The Open Chromatin Domains of Granulosa Cells Contain Stage-Specific DNA Sequence Motifs

(A) Predictive analysis of the top 10 motifs identified by HOMER as enriched in stage-specific open chromatin regions. Bar (lower y axis) and overlapping line plots (upper y axis) showing identified motifs count and their p value, respectively.

(B) Pie charts represent the percentage of stage-specific and common FAIRE peaks harboring LRH-1 motifs. Motif density plots show occurrence of the LRH-1/Nr5a2 motif in a window of ±0.5 kb around the FAIRE peak centers.

See also Figure S2 and Table S2.

has been shown that these transcription factors have the potential to modulate chromatin accessibility and collaborate with other nuclear receptors to establish a specific cell-type transcriptional network (Biddie et al., 2011; Madrigal and Alasoo, 2018; Vierbuchen et al., 2017).

Interestingly, our HOMER analysis also revealed that the LRH-1/Nr5a2 motif (core motif CAAGG) was among the most enriched in open chromatin, both before and following the OvS (Figures 2A and S2C; Table S2) suggesting its direct implication in the regulation of ovulation. More specifically, 24% (1,990 regions in +OvS) and 29% (2,195 regions in −OvS) of stage-specific FAIRE regions harbored the LRH-1 motif, demonstrating that nearly a quarter of all dynamic FAIRE sites are potentially bound by LRH-1. Thus, these results suggest LRH-1 is an important ovarian gene regulator present in differing chromatin regions before and after the OvS, strongly indicating a significant reprogramming of the LRH-1 cistrome.

Dynamic LRH-1 Cistrome Reprogramming Controls Granulosa Cell Differentiation

To better understand the role of LRH-1 in granulosa cells, we performed ChIP-seq analysis to define the LRH-1 cistrome before and after the OvS. Prior to the OvS, we identified 5,886 (1,948 −OvS-specific) LRH-1 binding sites whereas 9,413 (5,473 +OvS-specific) sites were found after the OvS, with 3,949 binding sites that were common to both stages (Figure 3A). These results are in agreement with the motif analysis of FAIRE predicting dynamic LRH-1 binding sites before and after the OvS and suggest that the OvS induces the chromatin remodeling that renders new DNA motifs accessible to LRH-1. Furthermore, *de novo* motif discovery analysis of LRH-1 binding sites identified a sequence that was very similar to the canonical LRH-1 motif (Figure 3B) and was comparable between stage-specific and common LRH-1 binding regions (Figure S2D). Motif analysis enrichment also revealed that the LRH-1 motif was co-enriched with AP-1 member's motifs after, but not before, the OvS, where it was more commonly associated with RAR, ER, and GATA motifs (Figure 3C; Table S2). These results are in keeping with FAIRE analysis, in which potential LRH-1 partner motifs follow the same pattern of enrichment.

As depicted in Figure 3D, the average signal of LRH-1 peaks specific to the −OvS stage decreased after the OvS, as did the FAIRE signal at the same stage (Figures 3D, S2E, and S2F). The LRH-1 binding sites that were common before and after the hormonal stimulus also exhibited perceptible chromatin remodeling that could be attributable to nuclear-receptor-mediated basal transcriptional repression (Santos et al., 2011). Inversely, the LRH-1-specific binding sites that increased following the OvS were correlated with a significant opening FAIRE signal at the same sites (Figures 3D, S2E, and S2F).

Furthermore, when we compared the LRH-1 binding sites with the FAIRE data, we found a large, but not complete, overlap. In fact, 54% of the LRH-1 binding sites overlapped the FAIRE peaks before the OvS and 42% overlapped with the FAIRE peaks thereafter (Figure 3E). If we only considered stage-specific regions, we established that 545 regions (28%) with a dynamic decrease in LRH-1 binding also had a dynamic closure chromatin before the OvS (Figures 3F, S2G, and S2H). Following the OvS, the LRH-1 binding increased in 1,035 regions with dynamic chromatin opening (19%) (Figures 3F, S2G, and S2H).

As an example, we found these results to be particularly convincing for *Star* and *Tnfaip6* (Figure 3G), two important regulators of steroidogenesis and cumulus expansion during folliculogenesis (Robker et al., 2018). Indeed, we observed that the LRH-1 signal coincided with the presence of more accessible DNA regions, both in proximity to the transcription start site

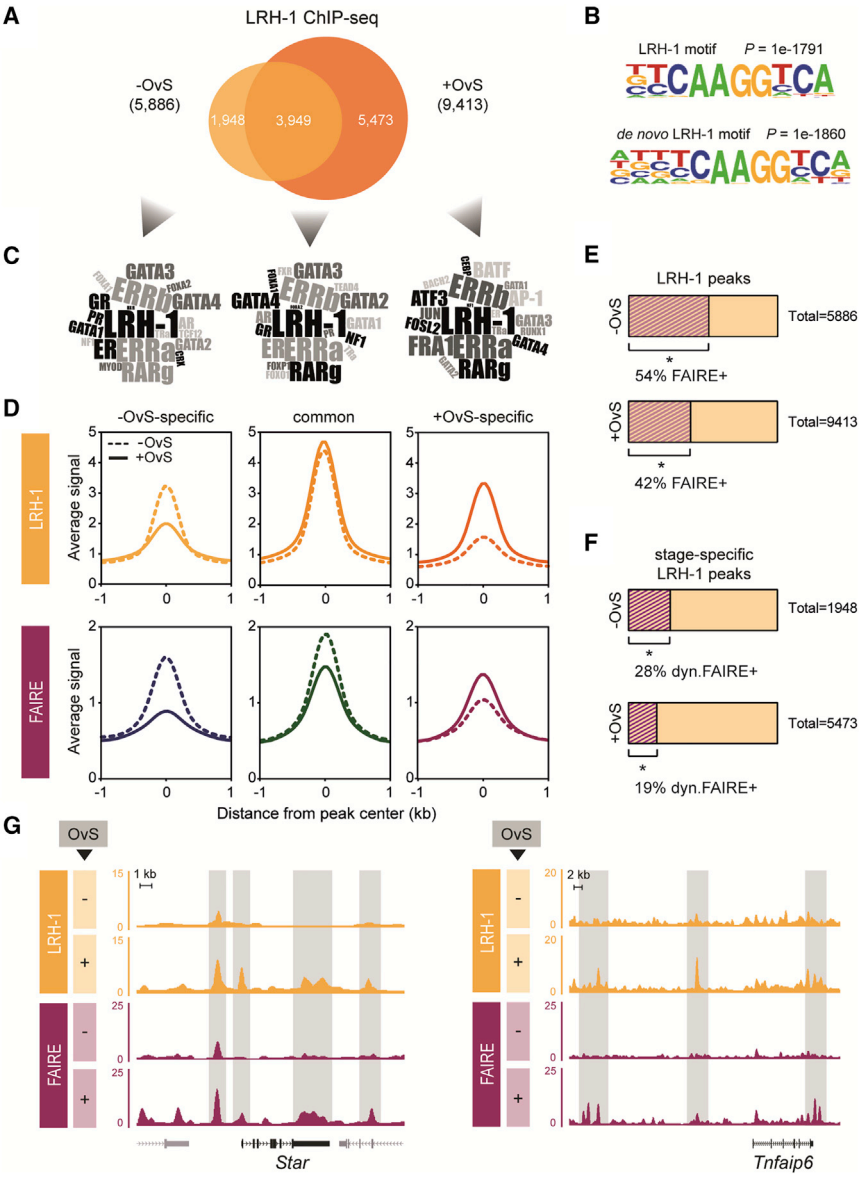

Figure 3. Dynamic LRH-1 Cistrome Reprogramming Controls Granulosa Cell Differentiation

(A) Venn diagram showing the LRH-1 cistrome before and after the OvS.

(B) Known and *de novo* LRH-1 motifs identified in +OvS LRH-1 binding sites. Similar motif was determined for common and −OvS-specific LRH-1 binding sites (see also Figure S2).

(C) Word clouds of top 20 predictive motifs across LRH-1 peak categories.

(D) Aggregated signal profiles of +OvS-specific, −OvS-specific, and common LRH-1 peaks in the 1-kb window around the peak center (upper panel) and the respective associated FAIRE signal for each cluster. The dotted line represents the LRH-1 or FAIRE signal before the OvS and the intact line represents the signal after the OvS.

(E) Bar plots showing the fraction of LRH-1 peaks that overlap with FAIRE peaks before and following the OvS.

(F) Bar plots showing the fraction of dynamic LRH-1 peaks that overlap dynamic FAIRE peaks before and following the OvS. p values indicate the significance for the overlap relative to genomic background (Fisher's exact test).

(G) UCSC Genome Browser tracks showing LRH-1 and FAIRE signals on two important ovarian genes, *Star* and *Tnfaip6*, during follicle differentiation. Grey boxes indicate the pronounced peaks and putative regulatory elements.

See also Figures S1 and S2 and Table S2.

(TSS) of these genes and in distal intergenic and intragenic domains. Together, these results demonstrate the plasticity of the LRH-1 cistrome following the OvS that controls differentiation at later stages of granulosa cells in their journey to luteinization.

An LRH-1 Transcriptional Switch Drives the Granulosa Cell Stage-Specific Gene Regulation Pattern

To further decipher the transcriptional events that take place around the OvS, we performed RNA sequencing (RNA-seq) evaluation of granulosa cells. First, we identified differentially expressed genes (DEGs; $p < 0.05$; fold change ≥ 2) in control mice (*Nr5a2*$^{f/f}$*Amhr2*$^{Cre-}$; CTL) before and after the OvS (Figure 4A; Table S3). As expected, expression of genes previously shown to be involved in processes that lead to ovulation and luteinization were induced after the OvS, for instance, *Pgr* for ovulation; *Ptx3, Areg*, and *Ereg* for cumulus expansion; and *Star* for steroidogenesis (Robker et al., 2018). Importantly, 30% of the +OvS DEGs were associated with one or more LRH-1 binding sites (Figure S3A; $p < 2.69e\text{-}16$), strongly suggesting a direct implication of LRH-1 in the regulation of specific pathways following the OvS. As expected, DEGs were significantly enriched in LRH-1 binding and FAIRE signal compared to non-DEG following the OvS (Figure S3B). Interestingly, these genes have been found to be over-represented in Gene Ontology (GO) terms related to differentiation and development processes, including those involved in cell migration (Figure S3C).

To focus on the more likely target genes of LRH-1 during ovulation, we then identified genes that are affected in granulosa cells of LRH-1 cKO mice (*Nr5a2*$^{f/f}$*Amhr2*$^{Cre+}$) before and after the OvS (Table S3). A global view of changes in gene expression is represented in Figures 4C and 4F. We found that the expression of a number of genes, including *Star* and *Tnfaip6*, which were increased in granulosa cells by the OvS in CTL, had a much reduced response in cKO mice, as shown in the RNA-seq University of California Santa Cruz (UCSC) tracks (Figure 4B). This is in agreement with previous published data showing a lower

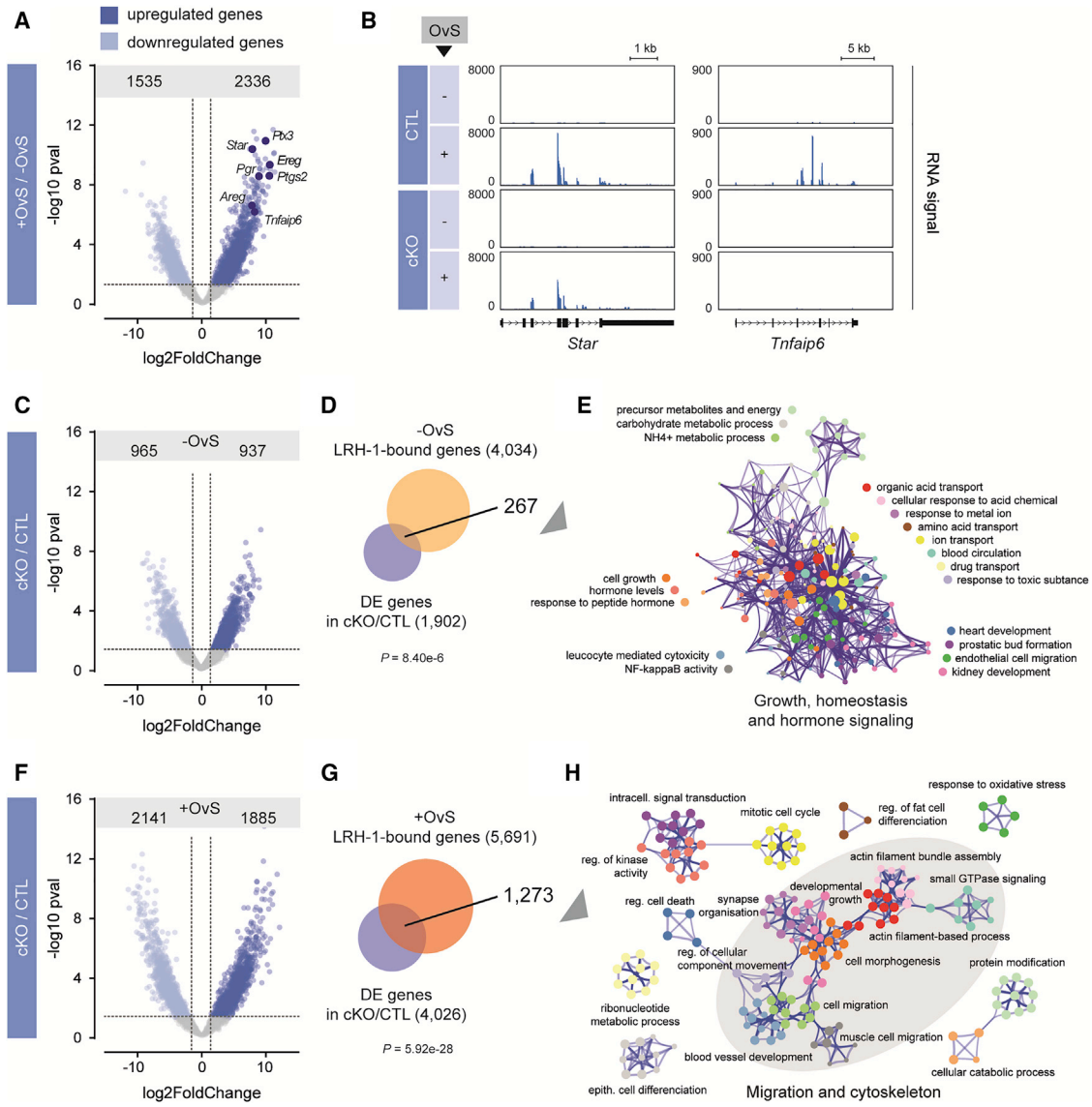

Figure 4. An LRH-1 Transcriptional Switch Drives the Granulosa Cell Stage-Specific Gene Regulation Pattern

(A) Volcano plot of RNA-seq signal in granulosa cells before and following the OvS in control (CTL) mice. Well-known regulators of follicle differentiation are highlighted.

(B) UCSC Genome Browser tracks showing mRNA expression profile on two important ovarian genes, *Star* and *Tnfaip6*, during follicle differentiation in CTL mice and LRH-1 cKO granulosa cells.

(C) Volcano plot of the RNA-seq signal in −OvS granulosa cells from LRH-1 cKO compared to CTL mice.

(D) Overlapping of −OvS-specific LRH-1-bound genes with DEGs in LRH-1 cKO compared to CTL granulosa cells. p value indicates significance of overlap (using the hypergeometric test).

(E) GO analysis of genes directly regulated by LRH-1 before the OvS with an emphasis on pathway associated with growth and hormone signaling.

(F) Volcano plot of RNA-seq signal of +OvS mouse granulosa cells in LRH-1 cKO compared to CTL.

(G) Overlapping of +OvS-specific LRH-1-bound genes with DEGs in LRH-1 cKO compared to CTL granulosa cells. p value indicates the significance of overlap (using the hypergeometric test).

(H) GO analysis of genes directly regulated by LRH-1 following the OvS, highlighting pathways associated with migration and cytoskeletal remodeling.

See also Figure S3 and Tables S3 and S4.

abundance of these transcripts in the absence of LRH-1 in granulosa cells (Bertolin et al., 2017). These results are also supported by the observation that these genes undergo significant chromatin remodeling following ovulatory stimulus and that LRH-1 binds directly these genes and controls their expression (Figure 3G). Before the OvS, we detected 1,902 DEGs ($p < 0.05$; fold change ≥ 2), of which 267 displayed one or more LRH-1 binding sites (Figures 4C and 4D). The presence of networks with very tight

knots in the GO analysis of these genes showed a significant enrichment of pathways regulating growth, development, homeostasis, and hormone signaling (Figure 4E; Table S4). Following the OvS, we observed a difference in RNA abundance for 4,026 genes in cKO granulosa cells when compared to CTL. Of the genes that varied, a remarkable 1,273 (almost one-third) were found to be concurrently bound by LRH-1 (Figures 4F and 4G). In addition, it is of note that almost 40% of these genes varied in response to the OvS (Figures S3A and S3D). Interestingly, GO analysis identified multiple pathways, in particular those associated with cell migration, cytoskeleton organization, and angiogenesis (Figure 4H; Table S4). These findings provide strong evidence for a switch of LRH-1 transactivation toward a new transcriptional program after the OvS, consistent with the preparation of granulosa cells for ovulation. Taken together, these results show that the LRH-1 transcriptional switch affects a multitude of key genes known or suspected to be involved in the transition of granulosa cells from a state of proliferation to a state of terminal differentiation following the OvS.

LRH-1 Governs Cell Motility and Cytoskeleton Remodeling of Granulosa Cells following the OvS

Cytoskeletal remodeling and cell motility were prominent among the GO terms that emerged from our analysis. To validate more specifically the implication of LRH-1 in these pathways following the OvS, we analyzed the genomic profiles of genes involved in cell migration that were detected by our ChIP-seq analysis, since these genes are expected to be directly regulated by LRH-1. Sequencing tracks and LRH-1 ChIP-qPCR validation showed new binding or enrichment of LRH-1 at genomic loci associated with genes such as *Akap2*, *Acvr1*, *Hs6st1*, *Cnp*, or *Scg2*, all of which are linked with the migration process (Figure 5A, upper panel, and Figure S5A). These results are consistent with the increased chromatin accessibility observed by FAIRE-seq analysis (Figure 5A, lower panel, and Figure S5A) and with our previous localization of most of these loci at distal genomic regions. To validate RNA-seq analyses, we next performed qRT-PCR on these genes before and after the OvS in CTL and cKO granulosa cells. We confirmed a reduced abundance of these gene transcripts induced by the OvS when LRH-1 was depleted (Figures 5B and S5B). To further explore the implication of LRH-1 in cell motility, we also characterized some phenotypic aspects of granulosa cells associated with the LRH-1 network. First, the capacity of granulosa cells to migrate was measured. Granulosa cells from CTL and LRH-1 cKO mice were extracted from follicle before and after the OvS and submitted to a Boyden chamber assay (Figure 5C). After the OvS, CTL granulosa cells massively crossed the porous membrane, whereas LRH-1 cKO cells were clearly unable to migrate (Figure 5D). Finally, using confocal immunofluorescence microscopy, we examined the cytoskeleton structure of granulosa cells from CTL and LRH-1 cKO mice. The OvS induced dramatic changes in the morphological structure of granulosa cells, as observed with the complete reorganization of the actin and tubulin networks (Figures 5E and S4). Indeed, granulosa cells became more spread rather than spheroid with signs of increased actin foci, redistribution of microtubules, and filopodia formation as shown in Figure 5F. In contrast, the cytoskeletal network of LRH-1 cKO granulosa cells was not reorganized, and no filopodia extension was observed. These results support the notion that LRH-1 plays a critical role in the cytoskeletal remodeling and migration of granulosa cells following the OvS, an essential step in the sequence to ovulation.

DISCUSSION

The surge of LH from the pituitary gland is the OvS that induces extensive remodeling of proliferating follicular granulosa cells as they proceed toward ovulation (Duggavathi and Murphy, 2009). These drastic morphological changes are driven by the genetic reprogramming of follicular cells to become terminally differentiated into luteal cells, a process that involves changes in the expression of hormone receptors and activation of multiple signaling pathways. Using an integrated genomic-transcriptomic approach, combining FAIRE-seq, ChIP-seq, and RNA-seq analysis in granulosa cells, we have defined a precise map of the transcriptional events that occur around the OvS.

We show here that the OvS induces extensive reprogramming of regulatory elements in granulosa cells, particularly those located in distal regions that are key effectors of enhancer activity for transcriptional regulation. Previous studies of genome-wide chromatin profiling have shown that enhancers are often located at large distances from gene promoters within the non-coding genome, communicating with promoters via chromatin looping mechanisms (Matharu and Ahituv, 2015). Those open chromatin regions distal to the gene promoter differ significantly between cell types and direct the correct spatiotemporal regulation of gene expression during development (Andrey and Mundlos, 2017; Heinz et al., 2015). Our FAIRE-seq results allowed us to define possible candidate granulosa cells stage-specific enhancers and to link distal regulatory elements to their potential target genes by *in silico* analysis. These findings elegantly reveal the regulatory elements that become more accessible following the OvS are associated to genes involved in several specific pathways indispensable for ovulatory processes, including TGF-β and gonadotropin signaling. Thus, chromatin structure analysis of long-range distal enhancers reveals the biological processes that characterize granulosa cell and tissue remodeling and lead to their specialization into luteal cells that occur after the OvS.

These data also highlight a DNA motif signature recognized by transcription factor networks that is predictive of the molecular determinants of the ovulatory processes. Indeed, our analysis revealed the presence of LRH-1 motifs both before and after the OvS and that there was a major shift in occupancy associated with the early stages of ovulation. LRH-1 is highly and exclusively expressed in murine granulosa cells, from the primordial follicles through all stages of follicular development, demonstrating a role for LRH-1 in all phases of folliculogenesis (Meinsohn et al., 2019). In agreement with our GO analysis before the OvS, LRH-1 regulates preovulatory proliferation of granulosa cells, as evidenced by its the expression of key genes that dictate the cell cycle, such as *Ccnd1*, *Ccnd2*, and *Cdkn1a* (Meinsohn et al., 2017). Furthermore, cKO of LRH-1 in granulosa cells has demonstrated unequivocally that this orphan nuclear receptor is required for fertility, and, in particular, these studies clearly

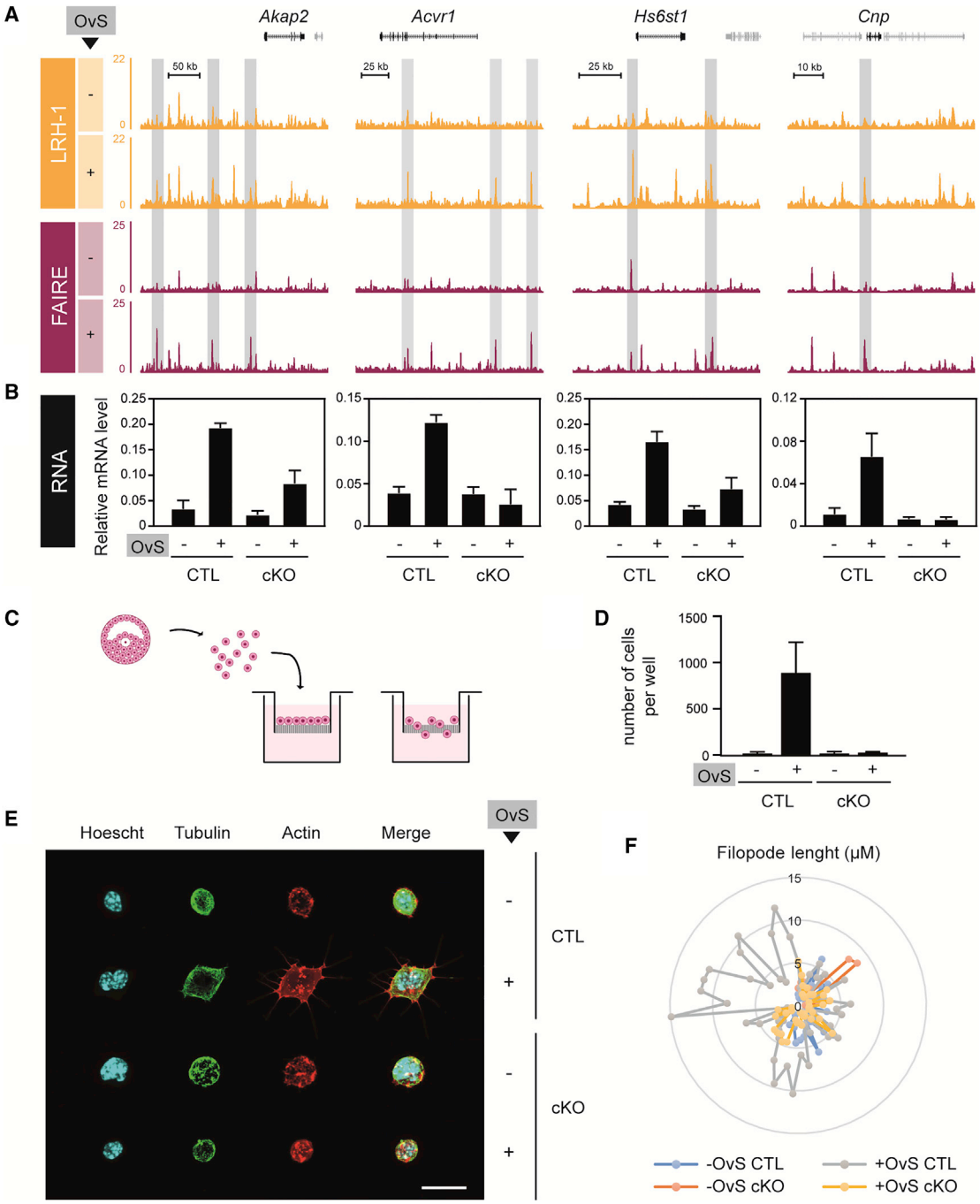

Figure 5. LRH-1 Governs Cell Motility and Cytoskeleton Remodeling of Granulosa Cells following the Ovulatory Signal

(A) UCSC Genome Browser tracks showing the remodeling pattern of LRH-1 binding by ChIP-seq and regulatory elements by FAIRE-seq of genes involved in cell migration, before and after the OvS. Gray boxes indicate dynamic regulatory regions.

(B) Gene expression analysis by qRT-PCR before and after the OvS in CTL or LRH-1 cKO granulosa cells. Data are expressed as mean ± SEM (n = 5).

(C) Schema of Boyden chamber cell migration experiment. Granulosa cells were extracted from ovary and plated on filter of a migration transwell.

(D) Quantification of the number of CTL or LRH-1 cKO granulosa cells extracted before and after the OvS migrating through the filter. Data are expressed as mean ± SD (n = 3).

(E) Representative images of cytoskeleton immunofluorescence comparing cKO and CTL granulosa cells. Cells aspirated from the ovary before and after the OvS were stained for cytoskeletal elements (actin in red with phalloidin and tubulin in green). Nuclei were labeled with Hoechst. Scale bar, 15 µM.

(F) Spider plot presenting the length of each filopodium identified and measured as distance between filopodial tip and cytoplasm edge for each condition (n = 4–5).

See also Figures S4 and S5 and Table S5.

establish that LRH-1 is indispensable for ovulation (Bertolin et al., 2014, 2017; Duggavathi et al., 2008).

Interestingly, our predictive transcription factor binding motif analysis before the OvS revealed the enrichment in GATA factors associated with the LRH-1 motif in open chromatin domains and LRH-1 binding regions. GATA transcription factors play important roles in cellular reprogramming to regulate cell fate specification and differentiation (Iwafuchi-Doi and Zaret, 2014; Pihlajoki et al., 2016). For instance, GATA transcription factors have been shown to cooperate as pioneer factors with other nuclear receptors, such as AR and ERα, to initiate specific transcriptional programs (Zaret and Carroll, 2011). Multiple GATA factors are expressed in granulosa cells, and it has been shown that these have redundant functions, since their simultaneous gene inactivation is necessary to cause infertility (Bennett-Toomey and Stocco, 2018). GATA-4 and GATA-6 granulosa double KO female mice fail to ovulate due to a lack of follicular development (Bennett et al., 2012). Indeed, GATA factors are known to regulate the expression of genes involved in follicle growth, such as *Ccnd2* and *Cdkn1a* and steroid synthesis (Convissar et al., 2015; Viger et al., 2008). These reports support our results suggesting that the GATA transcription factors are likely partners or pioneer factors driving LRH-1 to specific genomic regions involved in the regulation of cell cycle genes during the follicular development stage of the ovarian cycle.

We detected the LRH-1 binding motif in FAIRE sites present in both −OvS-specific and +OvS-specific open chromatin domains. These results suggest that newly accessible chromatin regions are bound by LRH-1 following an OvS, thereby revealing a reprogramming of the LRH-1 cistrome. We confirmed these results by ChIP-seq analysis by further demonstrating that LRH-1 is relocated to specific regions following the OvS. We validated LRH-1 as a direct regulator of *Star* and *Tnfaip6*, key genes in granulosa cell and ovulatory biology, by confirming LRH-1 binding at specific genomic regions that became more accessible in response to the OvS. Multiple molecular mechanisms could explain this LRH-1 transcriptional switch. First, LRH-1 is a constitutively active transcription factor, and the major regulators of its transactivational activity are the cofactors with which it interacts (Meinsohn et al., 2019). Therefore, the chromatin structural modifications induced by the LH surge involve not only LRH-1 but also its multiple partners, some of which allow for increased chromatin accessibility. Moreover, the OvS may trigger the activity of several intracellular signaling pathways in tandem that may affect LRH-1 by post-translational modifications to also modulate differential cofactor recruitment and transcriptional output (Meinsohn et al., 2019).

We found that the AP-1 transcription factor motifs are among the most enriched in open chromatin regions and LRH-1 binding sites following the OvS (Figures 2 and 3). Interestingly, specific members of the AP-1 family are regulated by follicle-stimulating hormone (FSH) and LH and exhibit different pattern of expression at different stages in follicular development (Sharma and Richards, 2000). Indeed, JunD and FRA2 are both rapidly induced following an LH surge correlating with the transition of proliferating granulosa cells to terminally differentiated luteal cells (Sharma and Richards, 2000). AP-1 has also been shown to act as a tethering factor for other transcriptional regulators such as ERα (Stender et al., 2010) or facilitate nuclear receptor binding by maintaining chromatin accessibility at regulatory elements (Biddie et al., 2011). Moreover, the involvement of AP-1 in cytoskeletal rearrangements, motility, and invasion in cancer cells (Liu et al., 2016; Zhao et al., 2014) is in keeping with massive remodeling of the LRH-1 cistrome and its biological effects following the OvS. In turn, this LRH-1 gene expression reprogramming of granulosa cells consequent to chromatin remodeling, potentially mediated by AP-1 factors, leads to terminal differentiation (Robker et al., 2018). This engenders the critical events in morphological remodeling of the follicle to support ovulation, including angiogenesis, cell motility, and cytoskeletal organization (Robker et al., 2018). In this study, we provide clear evidence that following the OvS, LRH-1 binds to specifically defined chromatin regions involved in regulating genes associated with these processes.

A rapid invasion of the previously avascular periovulatory follicle by the thecal blood vessels begins soon after the OvS and proceeds during process of luteinization (Murphy, 2000). Our GO analysis identified genes in granulosa cells that provoke angiogenesis and suggests that LRH-1 might also be a decisive regulator in this process. In support of this view, we have demonstrated herein that granulosa cells from LRH-1 cKO mice showed reduced abundance of transcripts involved in angiogenesis, such as *Vegfa*, *Pdgfb*, and *Slit2* (Figure S5B). These results are in agreement with histological analysis of LRH-1 cKO mice ovaries that reveal no sign of the invasion of the capillary network associated with differentiation into luteal cells (Duggavathi et al., 2008).

Confocal analysis shows that granulosa cells from LRH-1 cKO mice were unable to remodel their cytoskeleton following the OvS. These results corroborate the transcriptomic analysis showing that genes involved in cell motility and cytoskeleton were disrupted in LRH-1 granulosa cKO cells. Thus, our results establish more clearly the role of LRH-1 in granulosa cells physiology as a key player in cytoskeleton remodeling, an essential step of the ovulatory process (Kitasaka et al., 2018). It has been shown that cytoskeletal remodeling and cell migration are essential for the development of the corpus luteum (Becker et al., 2011; Franz et al., 2013; Rolaki et al., 2007). Further, modification of the cytoskeleton of cumulus cells is essential for their detachment and migration during expansion of the mouse cumulus-oocyte complex (Kitasaka et al., 2018). It has also been suggested that the cytoskeletal remodeling in mural granulosa cells participates in the downstream events leading to the rupture of the follicle (Grossman et al., 2015). Another important role of the cytoskeleton in the regulation of steroidogenesis has been reported (Sewer and Li, 2008). More particularly, it was shown that after the ovulatory stimulus in granulosa cells, a coordinated and precise regulation of vimentin, an important protein of the cytoskeleton, contributes to cholesterol transport and progesterone synthesis required for ovulation (Flynn et al., 2016; Shen et al., 2012). Together, these data are consistent with previous studies showing defective cumulus expansion and ovulation (Bertolin et al., 2014, 2017; Duggavathi et al., 2008) and disrupted progesterone production (Zhang et al., 2013) that are the sequelae to depletion of LRH-1 in granulosa cells.

As a general conclusion, the application of an integrated genomic and transcriptomic approach combining FAIRE-seq,

ChIP-seq, and RNA-seq analysis brings a better understanding of ovulatory processes, with an unprecedented depth in the characterization of the imperative and indispensable function of LRH-1 and its extensive regulatory network in the initiation of ovulation. Considering that LRH-1 is a nuclear receptor that can be targeted by agonists or antagonists, it has considerable potential for the regulation of fertility and the treatment of infertility.

STAR★METHODS

Detailed methods are provided in the online version of this paper and include the following:

- KEY RESOURCES TABLE
- LEAD CONTACT AND MATERIALS AVAILABILITY
- EXPERIMENTAL MODEL AND SUBJECT DETAILS
  - Mouse model
- METHOD DETAILS
  - Super stimulation protocol
  - FAIRE-sequencing
  - ChIP-sequencing
  - RNA-sequencing
  - RNA RTqPCR
  - Confocal immunofluorescence microscopy
  - Boyden chamber assay / migration assay
- QUANTIFICATION AND STATISTICAL ANALYSIS
- DATA AND CODE AVAILABILITY

SUPPLEMENTAL INFORMATION

Supplemental Information can be found online at https://doi.org/10.1016/j.celrep.2019.07.088.

ACKNOWLEDGMENTS

The authors thank Alain Lavigueur and Mylène Brunelle for critical comments on the article and helpful discussion. The authors also thank Fanny Morin, Vickie Roussel, Daniel Garneau, and Jean-Francois Lucier for technical assistance and Dominick Matteau and Sébastien Rodrigue for technical advice with RNA-seq. The authors are also grateful to Benoît Leblanc for the artwork for the graphical abstract. This work was supported by the Canadian Institutes of Health Research (CIHR; grant OGP12596 to N.G. and B.D.M). N.G. holds a Chercheur boursier (senior) award from the Fonds de recherche du Québec–Santé (FRQS).

AUTHOR CONTRIBUTIONS

S.B. and N.G. performed experimental work and analyzed the data. A.-M.B. and E.B. performed FAIRE-seq experiments. S.B., C.J.B., and A.D. completed RNA-seq analysis. S.B., B.D.M., and N.G. designed the study and wrote the manuscript.

DECLARATION OF INTERESTS

The authors declare no competing interests.

Received: December 18, 2018
Revised: May 1, 2019
Accepted: July 24, 2019
Published: August 27, 2019

REFERENCES

Andrey, G., and Mundlos, S. (2017). The three-dimensional genome: regulating gene expression during pluripotency and development. Development *144*, 3646–3658.

Arzate-Mejía, R.G., Recillas-Targa, F., and Corces, V.G. (2018). Developing in 3D: the role of CTCF in cell differentiation. Dev. Camb. Engl. *145*, dev137729.

Baby, V., Labroussaa, F., Brodeur, J., Matteau, D., Gourgues, G., Lartigue, C., and Rodrigue, S. (2018). Cloning and transplantation of the mesoplasma florum genome. ACS Synth. Biol. *7*, 209–217.

Becker, S., von Otte, S., Robenek, H., Diedrich, K., and Nofer, J.R. (2011). Follicular fluid high-density lipoprotein-associated sphingosine 1-phosphate (S1P) promotes human granulosa lutein cell migration via S1P receptor type 3 and small G-protein RAC1. Biol. Reprod. *84*, 604–612.

Bennett, J., Wu, Y.G., Gossen, J., Zhou, P., and Stocco, C. (2012). Loss of GATA-6 and GATA-4 in granulosa cells blocks folliculogenesis, ovulation, and follicle stimulating hormone receptor expression leading to female infertility. Endocrinology *153*, 2474–2485.

Bennett-Toomey, J., and Stocco, C. (2018). GATA regulation and function during the ovarian life cycle. Vitam. Horm. *107*, 193–225.

Bertolin, K., Gossen, J., Schoonjans, K., and Murphy, B.D. (2014). The orphan nuclear receptor Nr5a2 is essential for luteinization in the female mouse ovary. Endocrinology *155*, 1931–1943.

Bertolin, K., Meinsohn, M.C., Suzuki, J., Gossen, J., Schoonjans, K., Duggavathi, R., and Murphy, B.D. (2017). Ovary-specific depletion of the nuclear receptor Nr5a2 compromises expansion of the cumulus oophorus but not fertilization by intracytoplasmic sperm injection. Biol. Reprod. *96*, 1231–1243.

Bianco, S., Brunelle, M., Jangal, M., Magnani, L., and Gévry, N. (2014). LRH-1 governs vital transcriptional programs in endocrine-sensitive and -resistant breast cancer cells. Cancer Res. *74*, 2015–2025.

Bianco, S., Rodrigue, S., Murphy, B.D., and Gévry, N. (2015). Global mapping of open chromatin regulatory elements by formaldehyde-assisted isolation of regulatory elements followed by sequencing (FAIRE-seq). Methods Mol. Biol. *1334*, 261–272.

Biddie, S.C., John, S., Sabo, P.J., Thurman, R.E., Johnson, T.A., Schiltz, R.L., Miranda, T.B., Sung, M.H., Trump, S., Lightman, S.L., et al. (2011). Transcription factor AP1 potentiates chromatin accessibility and glucocorticoid receptor binding. Mol. Cell *43*, 145–155.

Binelli, M., and Murphy, B.D. (2010). Coordinated regulation of follicle development by germ and somatic cells. Reprod. Fertil. Dev. *22*, 1–12.

Bolger, A.M., Lohse, M., and Usadel, B. (2014). Trimmomatic: a flexible trimmer for Illumina sequence data. Bioinformatics *30*, 2114–2120.

Bray, N.L., Pimentel, H., Melsted, P., and Pachter, L. (2016). Near-optimal probabilistic RNA-seq quantification. Nat. Biotechnol. *34*, 525–527.

Brunelle, M., Coulombe, C., Poitras, C., Robert, M.A., Markovits, A.N., Robert, F., and Jacques, P.E. (2015). Aggregate and heatmap representations of genome-wide localization data using VAP, a versatile aggregate profiler. Methods Mol. Biol. *1334*, 273–298.

Convissar, S.M., Bennett, J., Baumgarten, S.C., Lydon, J.P., DeMayo, F.J., and Stocco, C. (2015). GATA4 and GATA6 knockdown during luteinization inhibits progesterone production and gonadotropin responsiveness in the corpus luteum of female mice. Biol. Reprod. *93*, 133.

Coulombe, C., Poitras, C., Nordell-Markovits, A., Brunelle, M., Lavoie, M.A., Robert, F., and Jacques, P.E. (2014). VAP: a versatile aggregate profiler for efficient genome-wide data representation and discovery. Nucleic Acids Res. *42*, W485–W493.

DeLuca, D.S., Levin, J.Z., Sivachenko, A., Fennell, T., Nazaire, M.D., Williams, C., Reich, M., Winckler, W., and Getz, G. (2012). RNA-SeQC: RNA-seq metrics for quality control and process optimization. Bioinformatics *28*, 1530–1532.

Duggavathi, R., and Murphy, B.D. (2009). Development. Ovulation signals. Science *324*, 890–891.

Duggavathi, R., Volle, D.H., Mataki, C., Antal, M.C., Messaddeq, N., Auwerx, J., Murphy, B.D., and Schoonjans, K. (2008). Liver receptor homolog 1 is essential for ovulation. Genes Dev. *22*, 1871–1876.

ENCODE Project Consortium (2012). An integrated encyclopedia of DNA elements in the human genome. Nature *489*, 57–74.

Fan, H.Y., Liu, Z., Johnson, P.F., and Richards, J.S. (2011). CCAAT/enhancer-binding proteins (C/EBP)-α and -β are essential for ovulation, luteinization, and the expression of key target genes. Mol. Endocrinol. *25*, 253–268.

Fayard, E., Auwerx, J., and Schoonjans, K. (2004). LRH-1: an orphan nuclear receptor involved in development, metabolism and steroidogenesis. Trends Cell Biol. *14*, 250–260.

Flynn, M.P., Fiedler, S.E., Karlsson, A.B., Carr, D.W., Maizels, E.T., and Hunzicker-Dunn, M. (2016). Dephosphorylation of MAP2D enhances its binding to vimentin in preovulatory ovarian granulosa cells. J. Cell Sci. *129*, 2983–2996.

Franz, M.B., Daube, S., Keck, C., Sator, M., and Pietrowski, D. (2013). Small GTPases are involved in sprout formation in human granulosa lutein cells. Arch. Gynecol. Obstet. *287*, 819–824.

Grossman, H., Chuderland, D., Ninio-Many, L., Hasky, N., Kaplan-Kraicer, R., and Shalgi, R. (2015). A novel regulatory pathway in granulosa cells, the LH/human chorionic gonadotropin-microRNA-125a-3p-Fyn pathway, is required for ovulation. FASEB J. *29*, 3206–3216.

Heinz, S., Benner, C., Spann, N., Bertolino, E., Lin, Y.C., Laslo, P., Cheng, J.X., Murre, C., Singh, H., and Glass, C.K. (2010). Simple combinations of lineage-determining transcription factors prime cis-regulatory elements required for macrophage and B cell identities. Mol. Cell *38*, 576–589.

Heinz, S., Romanoski, C.E., Benner, C., and Glass, C.K. (2015). The selection and function of cell type-specific enhancers. Nat. Rev. Mol. Cell Biol. *16*, 144–154.

Iwafuchi-Doi, M., and Zaret, K.S. (2014). Pioneer transcription factors in cell reprogramming. Genes Dev. *28*, 2679–2692.

Kaczynski, J., Cook, T., and Urrutia, R. (2003). Sp1- and Krüppel-like transcription factors. Genome Biol. *4*, 206.

Kim, J.B., Pjanic, M., Nguyen, T., Miller, C.L., Iyer, D., Liu, B., Wang, T., Sazonova, O., Carcamo-Orive, I., Matic, L.P., et al. (2017). TCF21 and the environmental sensor aryl-hydrocarbon receptor cooperate to activate a pro-inflammatory gene expression program in coronary artery smooth muscle cells. PLoS Genet. *13*, e1006750.

Kitasaka, H., Kawai, T., Hoque, S.A.M., Umehara, T., Fujita, Y., and Shimada, M. (2018). Inductions of granulosa cell luteinization and cumulus expansion are dependent on the fibronectin-integrin pathway during ovulation process in mice. PLoS ONE *13*, e0192458.

Li, H., and Durbin, R. (2010). Fast and accurate long-read alignment with Burrows-Wheeler transform. Bioinformatics *26*, 589–595.

Li, D., Liu, J., Yang, X., Zhou, C., Guo, J., Wu, C., Qin, Y., Guo, L., He, J., Yu, S., et al. (2017). Chromatin accessibility dynamics during iPSC reprogramming. Cell Stem Cell *21*, 819–833.e6.

Liu, X., Li, H., Rajurkar, M., Li, Q., Cotton, J.L., Ou, J., Zhu, L.J., Goel, H.L., Mercurio, A.M., Park, J.S., et al. (2016). Tead and AP1 coordinate transcription and motility. Cell Rep. *14*, 1169–1180.

Love, M.I., Huber, W., and Anders, S. (2014). Moderated estimation of fold change and dispersion for RNA-seq data with DESeq2. Genome Biol. *15*, 550.

Madrigal, P., and Alasoo, K. (2018). AP-1 takes centre stage in enhancer chromatin dynamics. Trends Cell Biol. *28*, 509–511.

Matharu, N., and Ahituv, N. (2015). Minor loops in major folds: enhancer-promoter looping, chromatin restructuring, and their association with transcriptional regulation and disease. PLoS Genet. *11*, e1005640.

McLean, C.Y., Bristor, D., Hiller, M., Clarke, S.L., Schaar, B.T., Lowe, C.B., Wenger, A.M., and Bejerano, G. (2010). GREAT improves functional interpretation of cis-regulatory regions. Nat. Biotechnol. *28*, 495–501.

Meinsohn, M.C., Morin, F., Bertolin, K., Duggavathi, R., Schoonjans, K., and Murphy, B.D. (2017). The orphan nuclear receptor liver homolog receptor-1 (Nr5a2) regulates ovarian granulosa cell proliferation. J Endocr Soc *2*, 24–41.

Meinsohn, M.-C., Smith, O.E., Bertolin, K., and Murphy, B.D. (2019). The orphan nuclear receptors steroidogenic factor-1 and liver receptor homolog-1: structure, regulation, and essential roles in mammalian reproduction. Physiol. Rev. *99*, 1249–1279.

Miyamoto, K., Nguyen, K.T., Allen, G.E., Jullien, J., Kumar, D., Otani, T., Bradshaw, C.R., Livesey, F.J., Kellis, M., and Gurdon, J.B. (2018). Chromatin accessibility impacts transcriptional reprogramming in oocytes. Cell Rep. *24*, 304–311.

Murphy, B.D. (2000). Models of luteinization. Biol. Reprod. *63*, 2–11.

Pepling, M.E. (2012). Follicular assembly: mechanisms of action. Reproduction *143*, 139–149.

Pihlajoki, M., Färkkilä, A., Soini, T., Heikinheimo, M., and Wilson, D.B. (2016). GATA factors in endocrine neoplasia. Mol. Cell. Endocrinol. *421*, 2–17.

Quinlan, A.R. (2014). BEDTools: the Swiss-army tool for genome feature analysis. Curr. Protoc. Bioinforma. *47*, 11.12.1–34.

Ramírez, F., Ryan, D.P., Grüning, B., Bhardwaj, V., Kilpert, F., Richter, A.S., Heyne, S., Dündar, F., and Manke, T. (2016). deepTools2: a next generation web server for deep-sequencing data analysis. Nucleic Acids Res. *44* (*W1*), W160–W165.

Risso, D., Ngai, J., Speed, T.P., and Dudoit, S. (2014). Normalization of RNA-seq data using factor analysis of control genes or samples. Nat. Biotechnol. *32*, 896–902.

Robinson, M.D., McCarthy, D.J., and Smyth, G.K. (2010). edgeR: a Bioconductor package for differential expression analysis of digital gene expression data. Bioinformatics *26*, 139–140.

Robker, R.L., Hennebold, J.D., and Russell, D.L. (2018). Coordination of ovulation and oocyte maturation: a good egg at the right time. Endocrinology *159*, 3209–3218.

Rolaki, A., Coukos, G., Loutradis, D., DeLisser, H.M., Coutifaris, C., and Makrigiannakis, A. (2007). Luteogenic hormones act through a vascular endothelial growth factor-dependent mechanism to up-regulate alpha 5 beta 1 and alpha v beta 3 integrins, promoting the migration and survival of human luteinized granulosa cells. Am. J. Pathol. *170*, 1561–1572.

Santos, G.M., Fairall, L., and Schwabe, J.W. (2011). Negative regulation by nuclear receptors: a plethora of mechanisms. Trends Endocrinol. Metab. *22*, 87–93.

Schindelin, J., Arganda-Carreras, I., Frise, E., Kaynig, V., Longair, M., Pietzsch, T., Preibisch, S., Rueden, C., Saalfeld, S., Schmid, B., et al. (2012). Fiji: an open-source platform for biological-image analysis. Nat. Methods *9*, 676–682.

Sewer, M.B., and Li, D. (2008). Regulation of steroid hormone biosynthesis by the cytoskeleton. Lipids *43*, 1109–1115.

Sharma, S.C., and Richards, J.S. (2000). Regulation of AP1 (Jun/Fos) factor expression and activation in ovarian granulosa cells. Relation of JunD and Fra2 to terminal differentiation. J. Biol. Chem. *275*, 33718–33728.

Shen, W.J., Zaidi, S.K., Patel, S., Cortez, Y., Ueno, M., Azhar, R., Azhar, S., and Kraemer, F.B. (2012). Ablation of vimentin results in defective steroidogenesis. Endocrinology *153*, 3249–3257.

Shin, H., Liu, T., Manrai, A.K., and Liu, X.S. (2009). CEAS: cis-regulatory element annotation system. Bioinformatics *25*, 2605–2606.

Simon, J.M., Giresi, P.G., Davis, I.J., and Lieb, J.D. (2012). Using formaldehyde-assisted isolation of regulatory elements (FAIRE) to isolate active regulatory DNA. Nat. Protoc. *7*, 256–267.

Stender, J.D., Kim, K., Charn, T.H., Komm, B., Chang, K.C., Kraus, W.L., Benner, C., Glass, C.K., and Katzenellenbogen, B.S. (2010). Genome-wide analysis of estrogen receptor alpha DNA binding and tethering mechanisms identifies Runx1 as a novel tethering factor in receptor-mediated transcriptional activation. Mol. Cell. Biol. *30*, 3943–3955.

Suske, G. (2017). NF-Y and SP transcription factors: new insights in a long-standing liaison. Biochim. Biophys. Acta. Gene Regul. Mech. *1860*, 590–597.

Svotelis, A., Gévry, N., and Gaudreau, L. (2009). Chromatin immunoprecipitation in mammalian cells. Methods Mol. Biol. *543*, 243–251.

Trapnell, C., Pachter, L., and Salzberg, S.L. (2009). TopHat: discovering splice junctions with RNA-Seq. Bioinformatics *25*, 1105–1111.

Vierbuchen, T., Ling, E., Cowley, C.J., Couch, C.H., Wang, X., Harmin, D.A., Roberts, C.W.M., and Greenberg, M.E. (2017). AP-1 transcription factors and the BAF complex mediate signal-dependent enhancer selection. Mol. Cell *68*, 1067–1082.e12.

Viger, R.S., Guittot, S.M., Anttonen, M., Wilson, D.B., and Heikinheimo, M. (2008). Role of the GATA family of transcription factors in endocrine development, function, and disease. Mol. Endocrinol. *22*, 781–798.

Ye, T., Krebs, A.R., Choukrallah, M.A., Keime, C., Plewniak, F., Davidson, I., and Tora, L. (2011). seqMINER: an integrated ChIP-seq data interpretation platform. Nucleic Acids Res. *39*, e35.

Yue, F., Cheng, Y., Breschi, A., Vierstra, J., Wu, W., Ryba, T., Sandstrom, R., Ma, Z., Davis, C., Pope, B.D., et al.; Mouse ENCODE Consortium (2014). A comparative encyclopedia of DNA elements in the mouse genome. Nature *515*, 355–364.

Zaret, K.S., and Carroll, J.S. (2011). Pioneer transcription factors: establishing competence for gene expression. Genes Dev. *25*, 2227–2241.

Zhang, Y., Liu, T., Meyer, C.A., Eeckhoute, J., Johnson, D.S., Bernstein, B.E., Nusbaum, C., Myers, R.M., Brown, M., Li, W., and Liu, X.S. (2008). Model-based analysis of ChIP-Seq (MACS). Genome Biol. *9*, R137.

Zhang, C., Large, M.J., Duggavathi, R., DeMayo, F.J., Lydon, J.P., Schoonjans, K., Kovanci, E., and Murphy, B.D. (2013). Liver receptor homolog-1 is essential for pregnancy. Nat. Med. *19*, 1061–1066.

Zhao, C., Qiao, Y., Jonsson, P., Wang, J., Xu, L., Rouhi, P., Sinha, I., Cao, Y., Williams, C., and Dahlman-Wright, K. (2014). Genome-wide profiling of AP-1-regulated transcription provides insights into the invasiveness of triple-negative breast cancer. Cancer Res. *74*, 3983–3994.

Zhou, Y., Zhou, B., Pache, L., Chang, M., Khodabakhshi, A.H., Tanaseichuk, O., Benner, C., and Chanda, S.K. (2019). Metascape provides a biologist-oriented resource for the analysis of systems-level datasets. Nat. Commun. *10*, 1523.

STAR★METHODS

KEY RESOURCES TABLE

REAGENT or RESOURCE	SOURCE	IDENTIFIER
Antibodies		
Mouse monoclonal anti-LRH-1	R and D Systems	Cat# PP-H2325; RRID:AB_2154053
Mouse monoclonal anti-α-Tubulin	Sigma-Aldrich	Cat# T9026; RRID:AB_477593
Goat anti-mouse Alexa 488	Molecular Probes (Invitrogen)	Cat# A-11029; RRID:AB_138404
Chemicals, Peptides, and Recombinant Proteins		
Dynabeads Protein A	Invitrogen	Cat# 10001D
Phalloidin-iFluor 555 Reagent	Abcam	Cat# ab176756
Deposited Data		
Raw and analyzed data	This paper	https://www.ncbi.nlm.nih.gov/geo/; GEO: GSE119508
Mus musculus genome assembly MGSCv37 (mm9)	Genome Reference Consortium	https://www.ncbi.nlm.nih.gov/assembly/GCF_000001635.18/
MOUSE (mm9) Blacklisted genomic regions	ENCODE Project Consortium	http://mitra.stanford.edu/kundaje/akundaje/release/blacklists/mm9-mouse/mm9-blacklist.bed.gz
DNaseI hypersensitive sites from mouse tissue	DNaseI Digital Genomic Footprinting from ENCODE/University of Washington [Mouse]	https://www.ncbi.nlm.nih.gov/geo/; GEO: GSE40869
Experimental Models: Organisms/Strains		
Mouse: C57BL/6 Nr5a2$^{f/f}$ Amhr2$^{Cre/-}$	Duggavathi et al., 2008	N/A
Mouse: C57BL/6 Nr5a2$^{f/f}$ Amhr2$^{Cre/+}$	Duggavathi et al., 2008	N/A
Oligonucleotides		
Primers for qPCR, see Table S5	This paper	N/A
Software and Algorithms		
Deeptools v3.2.0	Ramírez et al., 2016	https://deeptools.readthedocs.io/en/develop/; RRID:SCR_016366
Picard tool v1.64	Broad Institute	https://broadinstitute.github.io/picard/; RRID:SCR_006525
MACS2 v1.4 & v2.1.0	Zhang et al., 2008	https://github.com/taoliu/MACS/; RRID:SCR_013291
HOMER v4.7	Heinz et al., 2010	http://homer.ucsd.edu/homer/; RRID:SCR_010881
VAP v1.0.0	Coulombe et al., 2014	https://bitbucket.org/labjacquespe/vap/downloads/
CEAS v1.0.2	Shin et al., 2009	http://liulab.dfci.harvard.edu/CEAS/; RRID:SCR_010946
GREAT v3.0.0	McLean et al., 2010	http://great.stanford.edu/public/html/splash.php; RRID:SCR_005807
BWA v0.7.12	Li and Durbin, 2010	http://bio-bwa.sourceforge.net/; RRID:SCR_010910
Bedtools v2.27.1	Quinlan, 2014	https://bedtools.readthedocs.io/en/latest/; RRID:SCR_006646
Metascape	Zhou et al., 2019	http://metascape.org/gp/index.html#/main/step1; RRID:SCR_016620
TopHat v2.0.12	Trapnell et al., 2009	https://ccb.jhu.edu/software/tophat/index.shtml; RRID:SCR_013035
Kallisto v0.43.0	Bray et al., 2016	https://pachterlab.github.io/kallisto/about; RRID:SCR_016582

(*Continued on next page*)

Continued

REAGENT or RESOURCE	SOURCE	IDENTIFIER
RUVseq v1.10.0	Risso et al., 2014	https://bioconductor.org/packages/release/bioc/html/RUVSeq.html; RRID:SCR_006263
edgeR v3.26.4	Robinson et al., 2010	https://bioconductor.org/packages/release/bioc/html/edgeR.html; RRID:SCR_012802
DEseq2 v1.16.1	Love et al., 2014	https://bioconductor.org/packages/release/bioc/html/DESeq2.html; RRID:SCR_015687
GraphPad Prism	N/A	https://www.graphpad.com/; RRID:SCR_002798
R	N/A	https://www.r-project.org; RRID:SCR_001905

LEAD CONTACT AND MATERIALS AVAILABILITY

Further information and requests for resources and reagents should be directed to and will be fulfilled by the Lead contact, Nicolas Gévry (nicolas.gevry@usherbrooke.ca).

This study did not generate new unique reagents.

EXPERIMENTAL MODEL AND SUBJECT DETAILS

Mouse model

Animal experiments were approved by the University of Montreal Animal Care Committee and were conducted according to the guidelines of the Canadian Council on Animal Care. As described before (Bertolin et al., 2014; Meinsohn et al., 2017), mutant and control mice were maintained on a C57BL/6 background and were euthanized with isoflurane anesthesia, followed by cervical dislocation. LRH-1/Nr5a2 floxed (*Nr5a2*$^{f/f}$) mice have been described previously (Bertolin et al., 2014; Duggavathi et al., 2008). Granulosa-specific depletion of Nr5a2 from primary follicles was generated by crossing Nr5a2 floxed mice with mice expressing a Cre-recombinase driven by the anti-Müllerian type II receptor (*Amhr2*$^{Cre/+}$), gift of Dr. R. Behringer (Bertolin et al., 2014; Duggavathi et al., 2008) to produce conditional knockout (cKO) mice (genotype *Nr5a2* $^{f/f}$*Amhr2*$^{Cre/+}$). Control mice (CTL) in these trials were non mutant, *Nr5a2* $^{f/f}$*Amhr2*$^{Cre/-}$ females.

METHOD DETAILS

Super stimulation protocol

Ovarian stimulation was performed on 22 to 25 day old female mice by intraperitoneal injection of 5 IU equine chorionic gonadotropin (eCG; Folligon, Intervet) to stimulate follicular development, followed by the injection of 5 IU of human chorionic gonadodotropin (hCG; Chorulon, Intervet) 44 to 48 hours post-eCG treatment, to induce ovulation (Bertolin et al., 2014). For the following experiments, tissues from CTL and cKO mice were harvested 0, 4 and 8 hours after hCG treatments. After euthanasia, ovaries were collected and granulosa cells (GC) were isolated by ovarian puncture with 25 G needles in 1 mL of DMEM (Invitrogen). Oocytes were mechanically separated from the granulosa cells, which were then filtered with a 40-μM BD nylon Falcon Cell Strainer (Becton Dickinson) (Bertolin et al., 2014). Cells were immediately used for migration and cytoskeleton assays or pelleted, snap-frozen in liquid nitrogen and stored at –80°C for later experiments.

FAIRE-sequencing

Formaldehyde-Assisted Isolation of Regulatory Elements combined with sequencing (FAIRE-seq) experiments were essentially performed as previously described (Bianco et al., 2015). Briefly, to cross-link DNA-protein complexes, the resuspended granulosa cells pellets collected 0 and 4 hours post-hCG treatments (extracted from 8-10 ovaries per condition, performed in two independent experiments) were incubated for 10 minutes in 1X PBS/1.1% formaldehyde (Fisher) with a gentle stir at room temperature and fixing was arrested by adding glycine to a final concentration of 125 mM. Cells were then centrifuged (10 minutes, 900 x g, 4°C), washed with 1ml of 1X PBS with protease inhibitors, and centrifuged again (5 minutes, 12000 x g, 4°C). Fixed granulosa cells were resuspended in 200 μl of Lysis Buffer (1% SDS, 10 mM EDTA, 50 mM Tris pH 8.1) with protease inhibitors and incubated on ice for 30 minutes. For sonication, sample volume was adjusted to 500 μl with dilution buffer (0.01% SDS, 1.1% Triton, 1.2 mM EDTA, 16.7 mM Tris pH 8.1, 167 mM NaCl). Samples were sonicated with a Branson Ultrasonics Sonifier S-450 (Fisher Scientific) using an output of 2.75, duty cycle at 90% for 9 cycles of 10 pulses with 3 minutes on ice between each cycle, then centrifuged (10 minutes,

12000 x g, 4°C). PCI (Phenol/chloroform/isoamyl alcohol 25:24:1, Fisher Bioreagents) extraction was performed on supernatant as per manufacturer's protocol, except for the last centrifugation, which was done using phase lock gel (MaXtract Low density, QIAGEN). Samples were incubated for 16 hours at 65°C and DNA was purified using QIAquick PCR purification kit (QIAGEN) and quantified with a Nanodrop (Thermo Scientific). Next-generation sequencing libraries were constructed as previously described (Bianco et al., 2015) using 50 ng of DNA per sample. DNA fragment size and concentration were analyzed with High Sensitivity DNA kit on Bioanalyzer (Agilent) before sequencing. Illumina sequencing was performed by the BioMicro Center (Massachusetts Institute of Technology).

Sequencing reads of two independent replicates were aligned to the mouse reference genome mm9 using Burrows-Wheeler Aligner (BWA) (Li and Durbin, 2010) with default parameters. Only uniquely mappable reads with a mapping quality $\geq$ 10 were kept (above 70% of reads). Pearson correlation plots were generated with Deeptools (Ramírez et al., 2016) and the command-lines "multiBamSummary BED-file --BED --blackListFileName --ignoreDuplicates" and "plotCorrelation -c pearson -p scatterplot --removeOutliers --skipZeros" (Figure S1). After removing duplicate with Picard tool (http://broadinstitute.github.io/picard), peak calling was performed using Model-based Analysis for ChIP-Seq (MACS) (Zhang et al., 2008) with the parameters–nomodel and p value of 1e-4. Peaks belonging to chrM, chrY, unassembled random contigs and the mm9-blacklisted regions (ENCODE Project Consortium, 2012) were removed. Normalized read density was compiled using HOMER tool (Heinz et al., 2010) with the command-line "makeTagDirectory" and "makeUCSCfile" with default parameters (resolution 1 bp and normalization of the total number of reads to 1e7). Differentially accessible regions between before and after the OvS were defined using the edgeR R package (Robinson et al., 2010). Normalized reads were visualized using SeqMiner (Ye et al., 2011) and plotted profiles were obtained using Versatile Aggregate Profiler (VAP) (Brunelle et al., 2015; Coulombe et al., 2014) with the parameters "coordinate and absolute modes, 1 reference point and 40 windows of 50 bp." Genomic distributions were determined using Cis-regulatory Element Annotation System (CEAS) (Shin et al., 2009). Gene ontology (GO; biological processes and cellular component) and Molecular Signatures Database (MSigDB) pathway analyses were performed using Genomic Regions Enrichment of Annotations Tool (GREAT) (McLean et al., 2010). The top 5 of enriched and significant terms for each category was selected for the presentation in Figure 1. Nearby genes were assigned to FAIRE-seq peaks with parameter "single nearest gene: 1000 kb max extension, curated regulatory domains included" using GREAT. Motif discovery enrichment analysis was completed using the HOMER command findMotifsGenome.pl with parameter "-size 100." Motif density plot was generated with annotatePeaks.pl and "-m LRH1.motif -size 1000 -hist 50" parameters. Normalized UCSC (University of California, Santa Cruz) Genome Browser tracks were generated using HOMER as described above.

ChIP-sequencing

Given that LRH-1 is exclusively expressed in granulosa cells, ChIP experiments were performed on whole ovary, as described for other tissues (Svotelis et al., 2009) with some modifications. Briefly, ovarian tissues collected 0 and 4 hours post-hCG treatments (5 ovaries per condition, performed in two independent experiments) were washed in PBS, sliced in small pieces, and fixed for 15 minutes in 1X PBS/1.1% formaldehyde with agitation at room temperature. After adding glycine and washing with PBS, fixed tissues were incubated in lysis buffer and mechanically disrupted with an ice-cold Dounce. Chromatin was then sonicated in a Bioruptor apparatus (Diagenode) on "high"-intensity position for 30 s ON and 30 s OFF for 15 cycles at 4°C, cleared by a 10 minutes centrifugation at 10 000 x g. ChIP experiments were performed using 10μg of LRH-1 antibody with the use of magnetic protein A dynabeads (Life Technologies) for the immunoprecipitation. After washing, elution and crosslink reversion, samples were purified using a QIAquick PCR purification kit (QIAGEN) and quantified with PicoGreen assay (Invitrogen). Next-generation sequencing libraries were constructed as previously described (Bianco et al., 2015). DNA fragment size and concentration were analyzed with a High Sensitivity DNA kit on Bioanalyzer (Agilent) before sequencing. Illumina sequencing was performed on an Illumina HiSeq 2000 Sequencing system at the Plateau de biologie moléculaire et génomique fonctionnelle of the Institut de Recherche Cliniques de Montréal (IRCM).

ChIP-seq analysis was performed essentially as described above. Sequencing reads of two independent replicates with a mapping quality $\geq$ 20 were selected (82%–88% of aligned reads) and combined for subsequent analyses (Pearson correlation coefficients of 0.86, Figure S1). Peak calling was performed using MACS with q-value of 1e-2 (Zhang et al., 2008). MultiIntersectBed tool (Bedtools; (Quinlan, 2014)) was used to identify overlaps between LRH-1 ChIP-seq conditions or between LRH-1 and FAIRE peaks with parameter "-cluster." The significance for the overlap between LRH-1 and FAIRE-seq regions was measured relative to DNase I hypersensitive sites (DHSs; GSE40869 (Yue et al., 2014)) used as genomic background (Kim et al., 2017). Nearby genes were assigned to ChIP-seq peaks with parameter "single nearest gene: 1000 kb max extension, curated regulatory domains included" using GREAT and compared with differentially expressed genes from RNA-seq analysis for GO analysis using Metascape tool (Zhou et al., 2019). Enrichment network show the top 20 of significant biological processes terms.

RNA-sequencing

Total RNA of 3 distinct replicates from granulosa cells of CTL or LRH-1 cKO mice, at 0 and 4 hours post-hCG treatment, was extracted with RNeasy Mini Kits (QIAGEN) according to manufacturer instructions. RNA concentration was quantified by Nanodrop (Thermo Scientific). RNA quality control was performed with the RNA 6000 Nano Kit on Bioanalyzer (Agilent). All samples had an RNA Integrity Number (RIN) > 7.5. Sequencing libraries were prepared as previously described (Baby et al., 2018) with an input of

300 ng of total RNA. Libraries were analyzed and validated on a Bioanalyzer with High Sensitivity DNA kit (Agilent) before sequencing. Illumina sequencing was performed at the Plateau de biologie moléculaire et génomique fonctionnelle of the Institut de Recherche Cliniques de Montréal (IRCM).

Sequencing reads were filtered using Trimmomatic with parameters "ILLUMINACLIP:adapters.fa:2:30:15 TRAILING:30 MINLEN:32" (Bolger et al., 2014) and aligned to the mouse reference genome mm9 using TopHat (Trapnell et al., 2009). Quality control metrics were analyzed using RNA-SeQC (DeLuca et al., 2012). UCSC tracks were generated using HOMER tool as described above. Quantification of transcript abundance was performed using Kallisto (Bray et al., 2016) and generated data were normalized using Remove Unwanted Variation using control genes (RUVg) from RUVseq (Risso et al., 2014). The DESeq2 R package (Love et al., 2014) was then used to generate differential gene expression analysis.

RNA RTqPCR

Total RNA of 5 distinct replicates was extracted with RNeasy Mini Kits (QIAGEN) according to manufacturer instructions and was reverse transcribed into first-strand cDNA using M-MLV Reverse Transcriptase (Enzymatics) and random hexamer primers. Samples were subjected to qPCR with a CFX-96 Touch apparatus (Bio-Rad) using *Actβ* mRNA as internal control. Primers, listed in Table S5, were validated by standard curves and data were analyzed using the $2^{-\Delta CT}$ method.

Confocal immunofluorescence microscopy

Collagen (Sigma-Aldrich) was added to 8-well cover glass plates (Sarstedt) at a final concentration of 500 μg/mL. Plates were incubated at room temperature for a minimum of 1 hour, collagen solution was removed and plates were rinsed 4x with 1X PBS. Granulosa cells collected from cKO and CTL mice ovary at 0 and 8 hours post-hCG treatments were plated at ~$7x10^4$ cells/well in collagen-coated 8-well cover glass plates and incubated 15 minutes at 37°C. The supernatant containing unattached cells was removed and attached granulosa cells were fixed with 4% paraformaldehyde (PAF) (Sigma-Aldrich) in PBS at room temperature for 10 minutes. Following fixation, PAF was removed, replaced with 1X PBS and plates were sealed and conserved at 4°C. Cells were permeabilized 5 minutes in 1X PBS / 0.1% Triton, blocked in 1X PBS / 1% BSA during 30 minutes and incubated in α-tubulin primary antibody (1/500) (Sigma-Aldrich) during 60 minutes. Cells were washed three times in 1X PBS before a 60 minutes incubation with phalloidin-iFluor 555 reagent according to the manufacturer's protocols (Abcam), Hoechst 1/100 (stock solution 100 μg/ml) and Alexa Fluor 488 secondary antibody (1/500) (Invitrogen). Plates were washed as described above and analyzed using an Olympus FV3000 confocal microscope at 60x magnification. Length of the filopodia was measured as distance between filopodial tip and cell edge with FIJI (Schindelin et al., 2012). Antibodies used are listed in Table S5.

Boyden chamber assay / migration assay

Cell suspensions prepared for confocal immunofluorescence microscopy were centrifuged at 100 x g for 10 minutes at room temperature to obtain cells pellets that were resuspended in DMEM (Invitrogen) at a concentration of $1x10^5$ cells/mL. The Boyden chamber assay was performed by adding 1 mL of DMEM (Invitrogen) supplemented with 10% heat-inactivated-stripped-FBS (Thermo Scientific) in a 24-wells plate (Falcon). Boyden chambers (Greiner Bio-one) were added and granulosa cells were plated at $5x10^4$ cells/Boyden chamber and incubated at 37°C, 5% CO_2 for 26 hours. On the following day, all culture medium was removed and the interior of the Boyden chambers were cleaned with a cotton swab to remove the cells that did not migrate. The Boyden chambers were then washed once in 1X PBS, fixed with 4% formaldehyde in 1X PBS at room temperature for 20 minutes, washed twice in 1X PBS and kept in the last wash. Plates were finally sealed and conserved at 4°C before staining with Hoechst 1/100 (stock solution 100 μg/ml). Cells were examined and counted under a Zeiss Axio Observer Z1 fluorescence microscope.

QUANTIFICATION AND STATISTICAL ANALYSIS

All statistical analyses were performed using GraphPad Prism software and R package. *P*-values are indicated in Figures and Figure legends. For sequencing data, the sample size is indicated in Method details and represents the number of independent experiments. For FAIRE-seq analysis, differentially accessible regions were defined as FAIRE peaks that changed greater than twofold with a P-value < 0.02 using the edgeR R package. *P*-values for overlaps of two sets of genomic regions (FAIRE-seq and ChIP-seq) in a given genomic background were calculated using the Fisher's exact test. *P*-values for group comparisons of median (FAIRE-seq and ChIP-seq enrichment) were calculated using the non-parametric Wilcoxon test (paired) or the Mann–Whitney test (unpaired). For RNA-seq analysis, differentially expressed genes were defined by a fold change $\geq$ 2 (log2FC $\geq$ 1) and P-value < 0.05 using the DESeq2 R package. *P*-values to assess the significance of overlaps between two groups of genes were calculated using the hypergeometric test. For RT-qPCR, migration assay and immunofluorescence, the sample size n is indicated in the figure legends and represents the number of mice used for each condition. Data are expressed as mean ± SD or ± SEM.

DATA AND CODE AVAILABILITY

All genomic data in this publication have been deposited in NCBI's Gene Expression Omnibus and are accessible through GEO Series accession number GEO: GSE119508.